KRONOS FUSION ENERGY

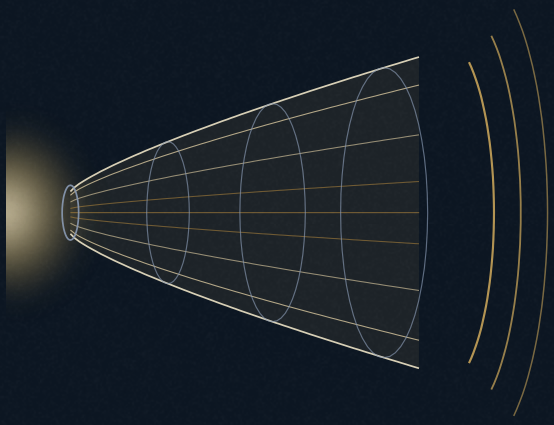

PAPER 2.29 · THE KRONOS 2026 SERIES

Component Activation, Waste-Class Routing, and Decommissioning of a Low-Activation Compact Spherical-Tokamak Breeder: No Isotope Beyond a Century's Half-Life

The environmental case for a fusion breeder is settled at end of life, in the activation it accumulates, the waste classes that inventory passes through as it cools, and the ease…

Read it live — 3-D model · physics validator · film series

BY P I FORD AND G L KULCINSKI

2026 · EDITORIAL EDITION

THE OFFICIAL RECORD

What this document is, and how to read its numbers

This is a combined editorial. It gathers, in one volume, the two design studies Kronos Fusion Energy released in 2026 — a compact spherical-tokamak tritium/helium-3 breeder and a deuterium–helium-3 tandem-mirror generator — together with the intellectual-property estate, the people, and, in the internal edition, the full commercial case. The scientific text is the same text that appears in the arXiv preprints and the journal submissions; the editorial adds the apparatus a reader needs to hold the whole program at once, and nothing in the physics is altered to fit it.

THE HONESTY STANCE IS THE ASSET

Every headline quantity carries an **evidence class** — DERIVED RECOMPUTED MEASURED REQUIREMENT — and, where a number is a modelled extrapolation rather than a demonstrated value, it is labelled as such and its downside is shown next to it. Several quantities in the underlying corpus moved after first publication; where a value has been withdrawn or restated, the record says so plainly. This is deliberate: a diligence team will find the load-bearing assumptions, so the document surfaces them first.

TWO EDITIONS

This volume is issued in two editions. The **public edition** (light) carries the physics and the design only — no dollar, price, or per-kilogram figure appears anywhere in it. The **internal edition** (dark) adds the economics, the funding architecture, and the defense-commercial analysis, and is marked *Confidential* accordingly; it is not for public distribution. Where the commercial case rests on a modelled assumption rather than a demonstrated one, it is labelled as such and its downside is shown alongside it, on the same terms as the physics.

TITLE	The Kronos Fleet — Hyperion · Aegis · MetroVolt: A Combined Design & Commercialization Study
AUTHOR	Priyanca Ford, Founder & CEO, on behalf of Kronos Fusion Energy
EDITION	2026 Combined Editorial · first issue
COMPANION WORKS	The five-paper arXiv drop — (1) Breeder, (2) Burner, (3) REBCO magnet & tape, (4) Direct Energy Conversion, (5) AI/ML/Quantum control — with matching numbered Zenodo deposits, plus the IOP journal and IAEA-FEC submissions. Patents were filed before the drop.
NAMING	Hyperion = the breeder; Aegis (defense) and MetroVolt (data-center) = one generator in two housings. Internal mode letters (D1, L) do not appear on public surfaces.
STATUS	Conceptual design & simulation study. Nothing herein is a construction commitment.

HOW TO READ THIS VOLUME

The fleet at a glance, and the way its numbers are marked

This volume opens with *Orientation*, presents the five research papers as a bound sequence, and closes with the *Apparatus*. *Foundations* sets out the three general results both machines rest on. *Paper One* is the Hyperion breeder; *Paper Two* the Aegis / MetroVolt generator; *Papers Three, Four and Five* are the enabling science — high-field REBCO magnets and tape, direct energy conversion, and the AI / ML / quantum control stack. A *Digital Twin & 3-D Model* part follows, then the *Environmental* profile. The *Economics* and levelized cost and the *Business Case* and diligence record appear in the internal edition only; the *Simulations* proof record and the Apparatus — patent portfolio, team, limitations, and sources — close both editions.

THE FLEET AT A GLANCE

	HYPERION	AEGIS	METROVOLT
Role	Strategic-isotope foundry	Defense installation power	Campus power
Machine	**Spherical tokamak**	**Tandem mirror**	**Tandem mirror**
Fuel	Deuterium–tritium	Deuterium–helium-3	Deuterium–helium-3
Delivers	Tritium · ^{3}He · 14 MeV n	Resilient installation power	Firm campus power
Physics bar	**Fusion gain only**	Closure (gates named)	Closure + lunar ^{3}He
In the fleet	Breeds the fuel	Proves the generator	Commercial destination

HOW THE NUMBERS ARE MARKED

Every headline quantity carries an evidence class — DERIVED from first principles, RECOMPUTED from raw data, MEASURED in hardware, or a REQUIREMENT yet to be met. Financial figures carry a case label and are confined to the internal (confidential) edition. Values that moved after first publication are shown as withdrawn or restated rather than quietly changed. A capability you can evaluate is one whose limits are on the page.

ABSTRACT

Component Activation, Waste-Class Routing, and Decommissioning of a Low-Activation Compact Spherical-Tokamak Breeder: No Isotope Beyond a Century's Half-Life

The environmental case for a fusion breeder is settled at end of life, in the activation it accumulates, the waste classes that inventory passes through as it cools, and the ease with which the machine is retired. We report a rigorous activation, waste-routing, and decommissioning account for the Kronos *Hyperion* breeder — a compact negative-triangularity spherical tokamak operating at $P_{\mathrm{fus}} = 85.04$ MW, $I_p = 9.66$ MA, $B_0 = 8$ T, with a 16.84 T high-temperature-superconducting centrepost. A first-wall neutron flux of 5.628×10^{14} at a wall load of $1.89\ \mathrm{MW\,m^{-2}}$ is tallied on a 175-group VITAMIN-J structure in a three-dimensional OpenMC model normalized to a fusion neutron source of $S_n = 3.02 \times 10^{19}\ \mathrm{n\,s^{-1}}$, and the resulting spectra drive a full-chain Bateman transmutation–decay inventory in alara/fispact-ii with per-component classification against the U.S. 10 CFR 61 waste rule. The result is unambiguous: at a two-full-power-year exposure *every activated component classifies at or below Class C, with no greater-than-Class-C (GTCC) waste*; the largest Class-C index anywhere in the build is the ceramic breeder at 9.4×10^{-3}, two orders of magnitude below the regulatory boundary, and only tritium retention pushes any stream above Class A. The qualified low-activation high-entropy-alloy structure follows a clean descent — intermediate-level at one year, low-level at ten, and clearable below regulatory concern at one hundred — with a *long-lived isotopic fraction of zero at every cooling time*, because the composition screen categorically excludes the ^{94}Nb, ^{93}Zr and molybdenum activation channels that keep conventional alloys intermediate-level indefinitely. The retired inventory is passively safe: decay heat is ≤ 62 at one year, two orders below fission post-shutdown densities with no melt-driving pathway, and the stored energies are small — 16.06 MJ of plasma thermal energy (≈ 3.8 kg TNT-equivalent) and a radiologically inert ~ 0.3 GJ of coil field energy. Decommissioning handles a modest, largely recyclable footprint of order 40 t of steel and $90\ \mathrm{m^3}$ of concrete per installed megawatt at a lifecycle intensity of $10\text{–}30\ \mathrm{gCO_2e\,kWh^{-1}}$. The clean end of life is not a mitigation bolted on afterward; it is a computed consequence of a deliberately clean material choice, and it closes.

Open-access deposit (code & data, CC BY 4.0): DOI 10.5281/zenodo.22645846 · Zenodo community *kronos_fusion_energy*. Explore it live: interactive 3-D model · physics validator.

Keywords: activation inventory · radioactive-waste routing · 10 CFR 61 classification · clearance · decommissioning · low-activation high-entropy alloys · rigorous two-step · lifecycle carbon · spherical-tokamak breeder

CONTENTS

Table of Contents

NOMENCLATURE

Symbols, units, and the names of things

Q	plasma (fusion) gain, P_{fus}/P_{aux}
Q_E	engineering gain, net electric out / recirculating in
H_{98}	confinement enhancement over the IPB98(y,2) scaling
Z_{eff}	effective ion charge
c_{ee}	electron–electron bremsstrahlung leading coefficient, 2.120022 (exact)
τ_E	energy confinement time
I_p	plasma current
R_0, a	major radius, minor radius
κ, δ	elongation, triangularity
β_N	normalized plasma beta (Troyon-normalized)
TBR	tritium breeding ratio
DEC	direct energy conversion
CF	plant capacity factor (availability)
FOAK / NOAK / BOAK	first / n^{th} / best of a kind
Hyperion	the ST breeder (internal: Mode D2)
Aegis	the generator, defense/installation housing (internal: Mode M)
MetroVolt	the generator, data-center housing (Mode M)

activation inventory; radioactive-waste routing; 10 CFR 61 classification; clearance; decommissioning; low-activation high-entropy alloys; rigorous two-step; lifecycle carbon; spherical-tokamak breeder

§ 1

Introduction

The public and regulatory case for fusion is decided less by the peak performance a machine reaches than by what it leaves behind. A device that produced abundant neutrons but a legacy of long-lived, deep-disposal waste would forfeit much of the advantage that motivates fusion in the first place. The activation inventory of the in-vessel components, the routing of that inventory through waste classes as it cools, and the ease with which the retired machine can be dismantled and its material recycled are therefore first-order design outputs, not post-hoc environmental book-keeping [2,4]. This is doubly true for a *compact* breeder intended for near-urban, distributed deployment, where the licensing posture and the decommissioning burden are gating commercial constraints [39].

The Kronos *Hyperion* breeder is a compact, high-field, negative-triangularity spherical tokamak whose canonical operating point is fixed by the Tier-2 design freeze at major radius $R_0 = 1.20$ m, aspect ratio $A = 2.5$, elongation $\kappa = 2.0$, triangularity $\delta = -0.30$, on-axis field $B_0 = 8$ T, plasma current $I_p = 9.66$ MA and fusion gain $Q = 3.076$, producing $P_{\mathrm{fus}} = 85.04$ MW with a 16.84 T peak field on a demountable, no-insulation REBCO centrepost [1,28,29]. The machine is designed as a strategic-materials platform — a 14 MeV neutron source for tritium breeding, helium-3 co-production and medical-isotope manufacture — rather than as a net-electric plant [32]. In that role the fast-neutron field that loads and activates every in-vessel component is the same field that breeds the fuel, so the activation and waste account is inseparable from the mission.

Prior art. Activation and waste classification for magnetic fusion has a mature methodology. The transmutation–decay inventory is solved from tabulated cross-sections and decay data with inventory codes such as fispact-ii [6] and alara [7], driven by neutron spectra from Monte Carlo transport (openmc [8], coupled to CAD geometry through dagmc [10]) on evaluated libraries such as ENDF/B-VIII.0 [9]. The European DEMO programme has established that reduced-activation ferritic–martensitic (RAFM) steels such as EUROFER-97 reach low-level or clearable inventories on century timescales provided impurity control suppresses the long-lived activation products [2,3,16,17], and that the residual waste class is frequently set not by the bulk structure but by trace elements and by tritium management [2,5]. The waste-classification arithmetic itself is codified in the U.S. Nuclear Regulatory Commission's 10 CFR 61.55 sum-of-fractions rule [13,14] and, for the clearable endpoint, in the IAEA clearance levels [15]. What has been missing for a compact, high-wall-load spherical-tokamak breeder is a transport-driven, per-component account tied to a frozen engineering design point and to a specific, first-principles-screened low-activation alloy family.

Contribution. This paper supplies that account. Our contributions are: (i) a self-contained derivation of the governing activation transport, transmutation–decay and waste-classification equations, cast as the formal problem solved here (Sec. 2); (ii) a three-dimensional, spectrum-resolved rigorous-two-step (R2S) computational methodology run on the Kronos NVIDIA GPU high-performance-computing (HPC) campaign, with explicit normalization, discretization and reproducibility controls (Sec. 3); (iii) a per-component activation and waste-class result at a two-full-power-year exposure showing no GTCC waste and a largest Class-C index of 9.4×10^{-3} (Sec. 4); (iv) a waste-routing timeline for the qualified high-entropy-alloy (HEA) structure — ILW at one year, LLW at ten, clearable at one hundred, long-lived fraction zero — contrasted quantitatively against dirty reference alloys; and (v) the passive-safety, stored-energy, fuel-footprint and lifecycle-carbon envelope that closes the decommissioning case. The alloy design that furnishes the clearable endpoint is developed in companion first-principles studies [33,34]; the spatially-resolved shutdown-dose twin and streaming/occupational-dose neighbours are reported separately [35,36]; the displacement-damage lifetime that sets the component-replacement cadence, and hence the mass flow through the decommissioning stream, is quantified in the first-wall and centrepost-life studies [37]; the tritium source term and accident case that dominate the operational (as opposed to end-of-life) radiological hazard are treated in the environmental and tritium-safety companion [38].

§ 2

Governing equations and the formal problem

The activation and waste problem couples three physics layers: neutron transport, which fixes the local flux and spectrum; transmutation–decay kinetics, which propagate the nuclide inventory through irradiation and cooling; and the regulatory classification functionals, which map that inventory to a waste class and a clearance time. We state each in turn and then define the formal problem.

NEUTRON TRANSPORT AND THE GROUP FLUX

The neutron field obeys the steady-state linear Boltzmann transport equation for the angular flux $\psi(\mathbf{r}, \mathbf{\Omega}, E)$,

$$\mathbf{\Omega}\cdot\nabla\psi + \Sigma_t(\mathbf{r}, E)\,\psi = \int_{4\pi}\int_0^{\infty} \Sigma_s(\mathbf{r}, \mathbf{\Omega}'\to\mathbf{\Omega}, E'\to E)\,\psi(\mathbf{r}, \mathbf{\Omega}', E')\,dE'\,d\mathbf{\Omega}' + S(\mathbf{r}, \mathbf{\Omega}, E),$$

with total and scattering macroscopic cross-sections Σ_t, Σ_s and a fixed fusion source $S = \frac{1}{4\pi}\,s(\mathbf{r})\,\chi(E)$ whose energy spectrum $\chi(E)$ is the $\mathbf{14.06}$ MeV D–T birth line broadened by the ion temperature. The quantity the activation calculation requires is the multigroup scalar flux, obtained by integrating ψ over angle and over the g-th energy bin of a group structure $\{E_g\}_{g=0}^{G}$,

$$\phi_g(\mathbf{r}) = \int_{E_g}^{E_{g-1}}\int_{4\pi} \psi(\mathbf{r}, \mathbf{\Omega}, E)\,d\mathbf{\Omega}\,dE, \qquad g = 1, \dots, G.$$

We solve Eq. 1 by Monte Carlo, which estimates ϕ_g as a track-length tally over simulated histories; the estimator is unbiased and its statistical error scales as $N_{\mathrm{hist}}^{-1/2}$. The tally is returned per source neutron and is placed on an absolute basis by the fusion source rate. Charged fusion products deposit their energy in the plasma, so the neutron source rate follows directly from the fusion power and the D–T energy release $Q_{\mathrm{DT}} = \mathbf{17.59}$ MeV:

$$S_n = \frac{P_{\mathrm{fus}}}{Q_{\mathrm{DT}}} = \frac{85.04\ \mathrm{MW}}{17.59\ \mathrm{MeV}} = 3.02 \times 10^{19}\ \mathrm{n\,s^{-1}},$$

one 14 MeV neutron per reaction. The absolute group flux is then $\Phi_g(\mathbf{r}) = S_n\,\phi_g(\mathbf{r})$, and the first-wall total flux evaluated on this basis is $\Phi_{\mathrm{FW}} = \mathbf{5.628 \times 10^{14}}$, of which $\mathbf{1.071 \times 10^{14}}$ lies above $\mathbf{10}$ MeV and $\mathbf{17.1\%}$ sits in the $\mathbf{14}$ MeV band.

TRANSMUTATION–DECAY KINETICS: THE BATEMAN SYSTEM

Under the spectrum-averaged flux the nuclide number densities $N_i(\mathbf{r}, t)$ evolve by the transmutation–decay (Bateman) system, in which each species is fed by decay and neutron-induced production from its precursors and depleted by its own decay and neutron absorption,

$$\frac{dN_i}{dt} = \sum_{j\neq i}\left(\lambda_{j\to i} + \bar{\phi}\,\bar{\sigma}_{j\to i}\right)N_j - \left(\lambda_i + \bar{\phi}\,\bar{\sigma}_i\right)N_i, \qquad \bar{\phi}\,\bar{\sigma}_{j\to i} = \sum_g \phi_g\,\sigma^g_{j\to i},$$

where λ_i is the decay constant, $\lambda_{j\to i}$ the branching-weighted decay rate from j to i, $\sigma^g_{j\to i}$ the group reaction cross-section (capture, $(n,2n)$, (n,p), (n,α), …), and the one-group collapse uses the transport spectrum of Eq. 2. Collecting the inventory into a vector $\mathbf{N} = (N_1, \dots, N_M)^{\mathsf{T}}$, Eq. 4 is the linear autonomous system

$$\frac{d\mathbf{N}}{dt} = \mathbf{A}\,\mathbf{N}, \qquad \mathbf{A} = \mathbf{A}_{\mathrm{dec}} + \bar{\phi}\,\mathbf{A}_{\mathrm{tr}},$$

with the sparse transmutation–decay matrix $\mathbf{A}$ carrying decay on $\mathbf{A}_{\mathrm{dec}}$ and flux-driven transmutation on $\mathbf{A}_{\mathrm{tr}}$. Its formal solution over a constant-flux interval is the matrix exponential

$$\mathbf{N}(t) = e^{\mathbf{A}t}\,\mathbf{N}(0).$$

A schedule of irradiation and cooling is composed by chaining such intervals: during irradiation $\bar{\phi} > 0$ so $\mathbf{A} = \mathbf{A}_{\mathrm{dec}} + \bar{\phi}\,\mathbf{A}_{\mathrm{tr}}$; during cooling $\bar{\phi} = 0$ so $\mathbf{A} = \mathbf{A}_{\mathrm{dec}}$ and the inventory relaxes purely by decay,

$$\mathbf{N}(t_{\mathrm{irr}} + \tau) = e^{\mathbf{A}_{\mathrm{dec}}\tau}\,e^{(\mathbf{A}_{\mathrm{dec}} + \bar{\phi}\,\mathbf{A}_{\mathrm{tr}})t_{\mathrm{irr}}}\,\mathbf{N}(0).$$

ACTIVITY, DECAY HEAT, AND THE PASSIVE-SAFETY CONDITION

The specific activity and the specific decay heat of a component of mass m follow from the inventory as

$$a(t) = \frac{1}{m}\sum_i \lambda_i N_i(t), \qquad \dot{q}(t) = \frac{1}{m}\sum_i \lambda_i N_i(t)\,\bar{E}_i,$$

where $\bar{E}_i = \bar{E}_i^{\alpha} + \bar{E}_i^{\beta} + \bar{E}_i^{\gamma}$ is the mean energy released per disintegration. The passive-safety ("walk-away") requirement is that the retired inventory cannot heat itself to a damage temperature faster than it can shed heat. Writing the volumetric decay power $q''' = \rho\,\dot{q}$, the adiabatic bound on the time to reach an allowable temperature rise $\Delta T_{\mathrm{allow}}$ is

$$\tau_{\mathrm{walk}} = \frac{\rho\, c_p\, \Delta T_{\mathrm{allow}}}{q'''} = \frac{c_p\, \Delta T_{\mathrm{allow}}}{\dot{q}},$$

which is an underestimate because it neglects conduction and re-radiation. In steady state a slab of half-thickness L radiating from its surface reaches an equilibrium surface temperature T_s set by

$$\varepsilon\,\sigma_S\left(T_s^4 - T_\infty^4\right) = q'''\,L,$$

with Stefan–Boltzmann constant σ_S and emissivity ε. The safety margin is the statement $T_s \ll T_{\mathrm{melt}}$; we evaluate both Eqs. 9–10 in Sec. 4.2. The decisive qualitative fact is structural: the fusion reaction rate scales as $n^2\langle\sigma v\rangle$ and collapses on any temperature or density excursion, so unlike fission there is no critical mass and no self-sustaining heat source to outrun the passive removal.

WASTE CLASSIFICATION AND THE CLEARANCE FUNCTIONAL

The regulatory disposition of the cooled inventory is a linear functional of the specific concentrations $C_i(t)$ (in the units of the rule, e.g. $\mathrm{Ci\,m^{-3}}$ or $\mathrm{nCi\,g^{-1}}$). The 10 CFR 61.55 sum-of-fractions indices for the Class-A and Class-C boundaries are

$$\mathcal{I}_{\mathrm{A}}(t) = \sum_i \frac{C_i(t)}{L_i^{\mathrm{A}}}, \qquad \mathcal{I}_{\mathrm{C}}(t) = \sum_i \frac{C_i(t)}{L_i^{\mathrm{C}}},$$

evaluated over both the long-lived (Table 1) and short-lived (Table 2) nuclide sets, with $L_i^{\mathrm{A}}, L_i^{\mathrm{C}}$ the tabulated concentration limits. A stream is Class A if $\mathcal{I}_{\mathrm{A}} \le 1$, Class C if $\mathcal{I}_{\mathrm{C}} \le 1$, and greater-than-Class-C (requiring deep geological disposal) if $\mathcal{I}_{\mathrm{C}} > 1$. The clearable endpoint is governed by the analogous IAEA clearance index

$$\mathcal{I}_{\mathrm{clr}}(t) = \sum_i \frac{C_i(t)}{\mathrm{CL}_i} \le 1,$$

where CL_i is the clearance level below regulatory concern. Finally, the property that distinguishes a clean material from a merely diluted one is the *long-lived isotopic fraction* — the share of the activity carried by nuclides whose half-life exceeds a century,

$$f_{\mathrm{LL}}(t) = \frac{\displaystyle\sum_{i:\, t_i^{1/2} > 100\ \mathrm{yr}} \lambda_i N_i(t)}{\displaystyle\sum_i \lambda_i N_i(t)}.$$

A material with $f_{\mathrm{LL}} \to 0$ decays to clearance in finite time; one with $f_{\mathrm{LL}} \to 1$ (as for the ^{94}Nb / ^{93}Zr-bearing reference alloys) is trapped above clearance indefinitely regardless of cooling. This single scalar, and not the peak activity, is the target of the composition screen.

SHUTDOWN DOSE: THE RIGOROUS-TWO-STEP COUPLING

The occupational hazard during maintenance and decommissioning is the shutdown photon field, computed by the rigorous-two-step (R2S) method: the transport flux of Eq. 2 drives the activation of Eq. 4; the cooled inventory defines a decay-photon volumetric source

$$q_\gamma(\mathbf{r}, E_\gamma, t) = \sum_i \lambda_i N_i(\mathbf{r}, t)\, I_{\gamma,i}(E_\gamma),$$

with $I_{\gamma,i}$ the photon emission yield per decay; and a second transport solve of q_γ gives the shutdown dose-rate field $\dot{D}(\mathbf{r}, t)$. The contact-dose proxy used for component ranking is $\dot{D}_{\mathrm{contact}} \propto \sum_i A_i \bar{E}_{\gamma,i}$.

THE FORMAL PROBLEM

Given the frozen design point $\{R_0, A, \kappa, \delta, B_0, I_p, Q, P_{\mathrm{fus}}\}$, the material compositions $\{x_e\}$ of each in-vessel zone, an evaluated nuclear-data library $\{\sigma^g_{j\to i}, \lambda_i, \bar{E}_i\}$, and an irradiation/cooling schedule, *find* the per-component activity $a(t)$, decay heat $\dot{q}(t)$, waste indices $\mathcal{I}_{\mathrm{A}}(t), \mathcal{I}_{\mathrm{C}}(t)$, clearance time $t^\star$ at which $\mathcal{I}_{\mathrm{clr}} \le 1$, and long-lived fraction $f_{\mathrm{LL}}(t)$; and *certify* the design constraint

$$\boxed{\max_{\text{components}} \mathcal{I}_{\mathrm{C}}(t) \;\le\; 1 \quad \forall\, t \quad \text{and} \quad f_{\mathrm{LL}}(t) = 0 \quad \forall\, t,}$$

i.e. no GTCC waste at any cooling time and a vanishing long-lived fraction. Equation 15 is the statement this paper closes.

§ 3

Computational methodology: the GPU HPC campaign

The results below were produced on the Kronos NVIDIA GPU HPC campaign, the same in-house high-performance-computing estate (NVIDIA A100 / H100 / A10-class accelerators, with a petabyte object store for raw histories) that carries the company's coupled-twin and multi-physics workload [1,35]. The activation pipeline is a transport-then-inventory R2S chain (Fig. 1); we describe its geometry, discretization, solver and reproducibility controls, and where each stage is accelerated.

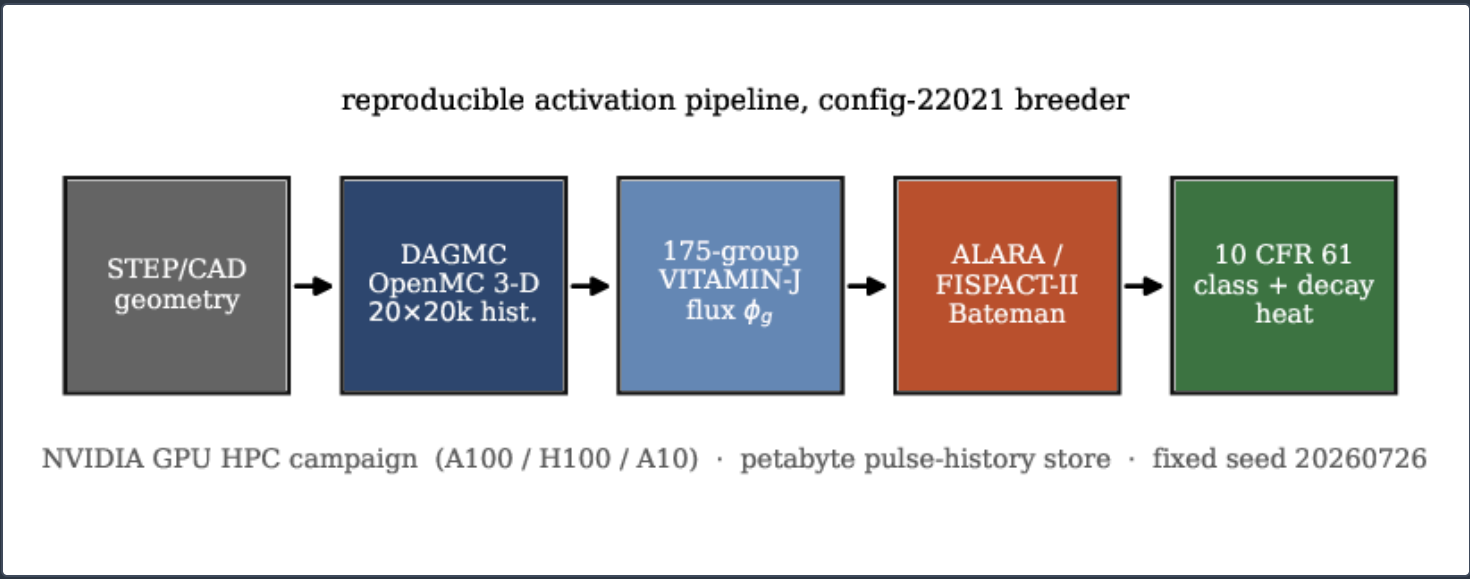

(Schematic.) The reproducible activation pipeline. CAD geometry is imported through dagmc into a three-dimensional openmc Monte Carlo transport solve ($20 \times 20{,}000$ histories) that tallies a 175-group VITAMIN-J flux; the spectrum-collapsed cross-sections drive the Bateman transmutation–decay solve in alara/fispact-ii, yielding per-component activity, decay heat, and 10 CFR 61 waste indices. The whole chain runs on the NVIDIA GPU HPC campaign under a fixed random seed.

TRANSPORT MODEL AND DISCRETIZATION

Neutron transport (Eq. 1) is solved with the continuous-energy Monte Carlo code openmc [8] on the ENDF/B-VIII.0 evaluation [9], with CAD-faithful geometry supplied through the Direct-Accelerated-Geometry Monte Carlo (dagmc) toolkit [10] so that the tallied spectrum reflects the true three-dimensional first-wall/blanket configuration rather than an idealized slab; the CAD-to-transport reproduction of the net breeding ratio is reported separately [35]. The flux is tallied on the 175-group VITAMIN-J energy structure — the standard fusion activation group set — resolving the **14** MeV line and the fast tail that drive threshold reactions. Two model fidelities are used and cross-checked: (i) a full three-dimensional tally in the P3 geometry with $\mathbf{20 \times 20{,}000}$ neutron histories (batches × particles/batch), used to fix the R2S source spectra and the absolute normalization; and (ii) a two-zone plane-slab inventory model (Fig. 2), a **3** cm EUROFER-97 first wall backed by a **50** cm breeder zone (**12 vol%** EUROFER + **14.74 vol%** Be multiplier + **34.40 vol%** $\mathbf{Li_4SiO_4}$ enriched to **90%** ^{6}Li), used for the extended-fluence per-component classification. The two fidelities agree on the trajectory and on the class assignment.

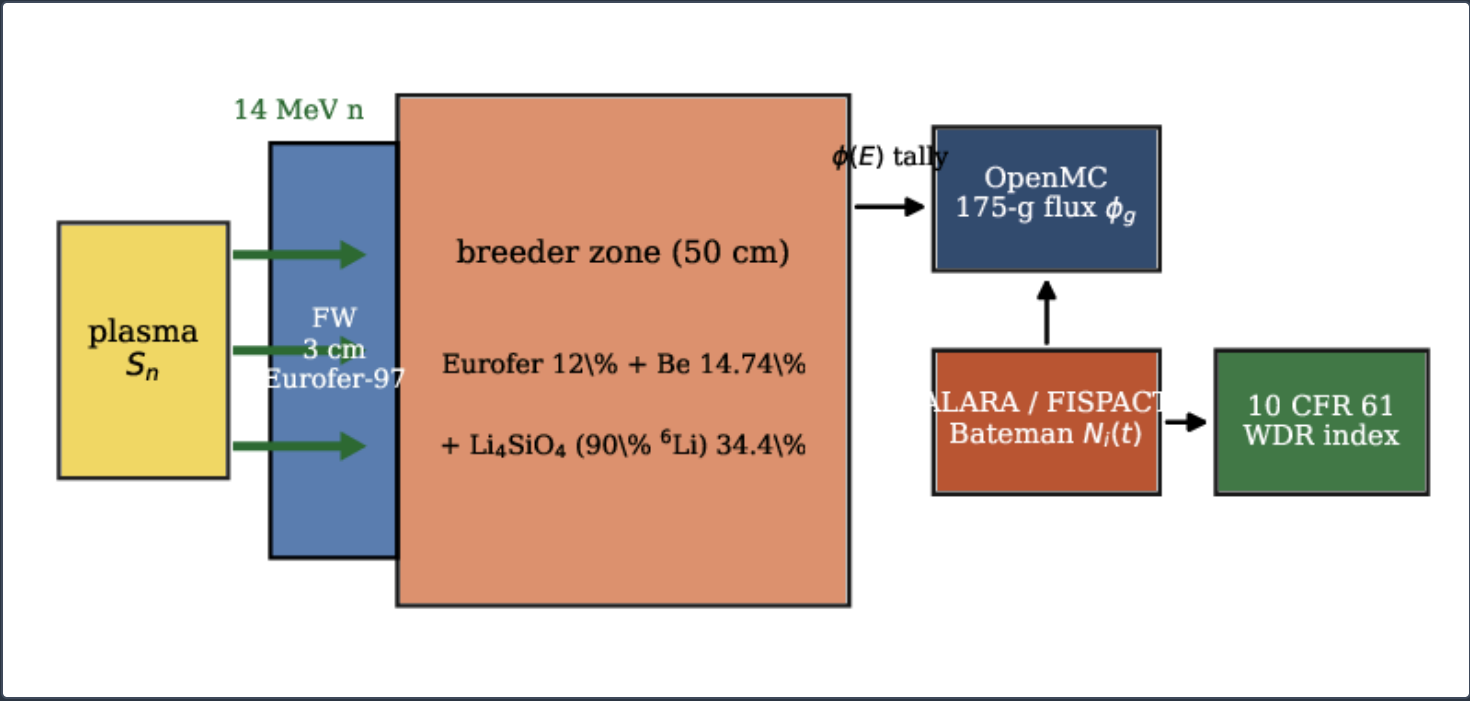

(Schematic.) The two-zone activation model. A 14 MeV fusion source of strength $S_n = 3.02 \times 10^{19}$ × area illuminates a **3** cm EUROFER-97 first wall and a **50** cm ceramic-breeder zone; the tallied VITAMIN-J spectrum feeds the Bateman solve and the 10 CFR 61 waste-detriment-response (WDR) classification.

ABSOLUTE NORMALIZATION

The Monte Carlo tally is per source neutron; the physical flux uses the fusion source rate of Eq. 3. As an independent check the uncollided-current estimate at the quoted wall load of $\mathbf{1.89\ MW\,m^{-2}}$ gives 8.39×10^{13} , consistent with the tallied first-wall value once in-scattered contributions are included. The breeder-zone total flux is 1.302×10^{14} . All inventory results are reported per unit mass directly from the code's per-mass output, avoiding a density-dependent $\mathbf{Ci\,m^{-3}} \rightarrow$ $\mathbf{Bq\,kg^{-1}}$ conversion.

INVENTORY SOLVER AND CONVERGENCE

The transmutation–decay system (Eq. 5) is integrated with alara [7], whose adaptive linear-chain expansion truncates each production–decay chain at a relative contribution of 10^{-7}, with independent cross-validation against the matrix-exponential inventory of fispact-ii [6]. The matrix exponential of Eq. 6 is evaluated by the Chebyshev Rational Approximation Method (CRAM), whose order-k partial-fraction form

$$e^{At} N_0 \approx \alpha_0 N_0 + 2\,\mathrm{Re}\sum_{\ell=1}^{k/2} \alpha_\ell \left(At - \theta_\ell I\right)^{-1} N_0,$$

with complex poles θ_ℓ and residues α_ℓ, is accurate to machine precision on the near-real negative spectrum characteristic of burnup matrices and is unconditionally stable across the extreme stiffness (half-lives spanning sub-second to 10^6 yr) of Eq. 4. The two solvers agree on all one-full-power-year trajectories and scale as expected between one- and two-full-power-year exposures. The irradiation schedule is a constant-flux steady irradiation (one and two full-power years) followed by a cooling grid at **1 s**, **1 d**, **100 d**, **1 yr**, **10 yr** and **100 yr**, with per-component (“constituent”) classification so that structural EUROFER, the Be multiplier and the ceramic breeder are classed separately against 10 CFR 61 Class-A and Class-C waste-detriment-response files.

GPU ACCELERATION AND REPRODUCIBILITY

The Monte Carlo transport — by far the dominant cost — is the stage that benefits from the GPU HPC campaign: history batches are distributed across the accelerator fleet, the petabyte store holds the raw and tallied histories, and the offline throughput (hours per campaign) sets the cadence at which the R2S spectra are refreshed. The inventory solve of Eq. 16 is comparatively inexpensive and runs on the same nodes. Every run in this paper is executed under a fixed random seed (`20260726`) on the config-22021 breeder design point; the transport tallies, the collapsed cross-sections, the inventory tables and the waste-classification indices are archived so that the entire chain regenerates deterministically. No compute-cost figures enter the physics; the campaign is described only by its codes, scale and reproducibility. The design point, materials, and model setup are collected in Table 1.

QUANTITY	VALUE	NOTE
major radius R_0	**1.20** m	compact ST
aspect ratio A	**2.5**	
elongation κ	**2.0**	
triangularity δ	**−0.30**	negative
on-axis field B_0	**8** T	
peak centrepost field	**16.84** T	REBCO, demountable
plasma current I_p	**9.66** MA	
fusion gain Q	**3.076**	
fusion power P_{fus}	**85.04** MW	D–T
neutron source S_n	$\mathbf{3.02 \times 10^{19}\ n\,s^{-1}}$	Eq. 3
first-wall neutron flux	$\mathbf{5.628 \times 10^{14}}$	**17.1%** in 14 MeV band
wall load	$\mathbf{1.89\ MW\,m^{-2}}$	
first wall	**3** cm EUROFER-97 (**93.33 vol%**)	W/Ta armour excluded
breeder zone	EUROFER **12%** + Be **14.74%** + Li_4SiO_4 **34.40%**	**90%** ^{6}Li
transport code	openmc + dagmc	ENDF/B-VIII.0

table continued

group structure	175-group VITAMIN-J	20×20k histories
inventory code	alara / fispact-ii	CRAM, chain trunc. 10^{-7}
classification	NRC 10 CFR 61.55	Class-A / Class-C WDR

§ 4

Results

ACTIVATION INVENTORY AND ITS DECAY

Figure 3 and Table 2 give the specific-activity trajectories. The EUROFER first wall falls from 3.13×10^{14} at shutdown to 1.15×10^{14} at one year and 4.97×10^{7} at one hundred years at the two-full-power-year exposure; the transport-driven one-full-power-year R2S model gives a consistent $2.64 \times 10^{14} \rightarrow 7.13 \times 10^{13} \rightarrow 2.70 \times 10^{7}$. The breeder zone starts at 1.83×10^{14} and drops 39% within the first second as the prompt ^{8}Be/^{6}He activity in the beryllium multiplier decays, reaching 7.69×10^{13} at one year. Its hundred-year residue of 2.76×10^{11} is *entirely bred tritium* held in the ceramic under a no-purge accounting convention; with tritium recovered as product — as it is in operation — the ex-tritium breeder inventory is 1.71×10^{14} at shutdown and only $\sim 4.5 \times 10^{6}$ at one hundred years. The shutdown inventory is dominated by short-lived ^{56}Mn and ^{52}V; the one-day-to-one-year window by ^{55}Fe, ^{54}Mn, ^{51}Cr and ^{49}V; and the hundred-year residue by ^{3}H and ^{53}Mn with trace ^{14}C and ^{10}Be. Every one of these is a short- or medium-lived species or a tritium term managed within the fuel cycle: the inventory contains no isotope that persists beyond a century's half-life in the structural stream.

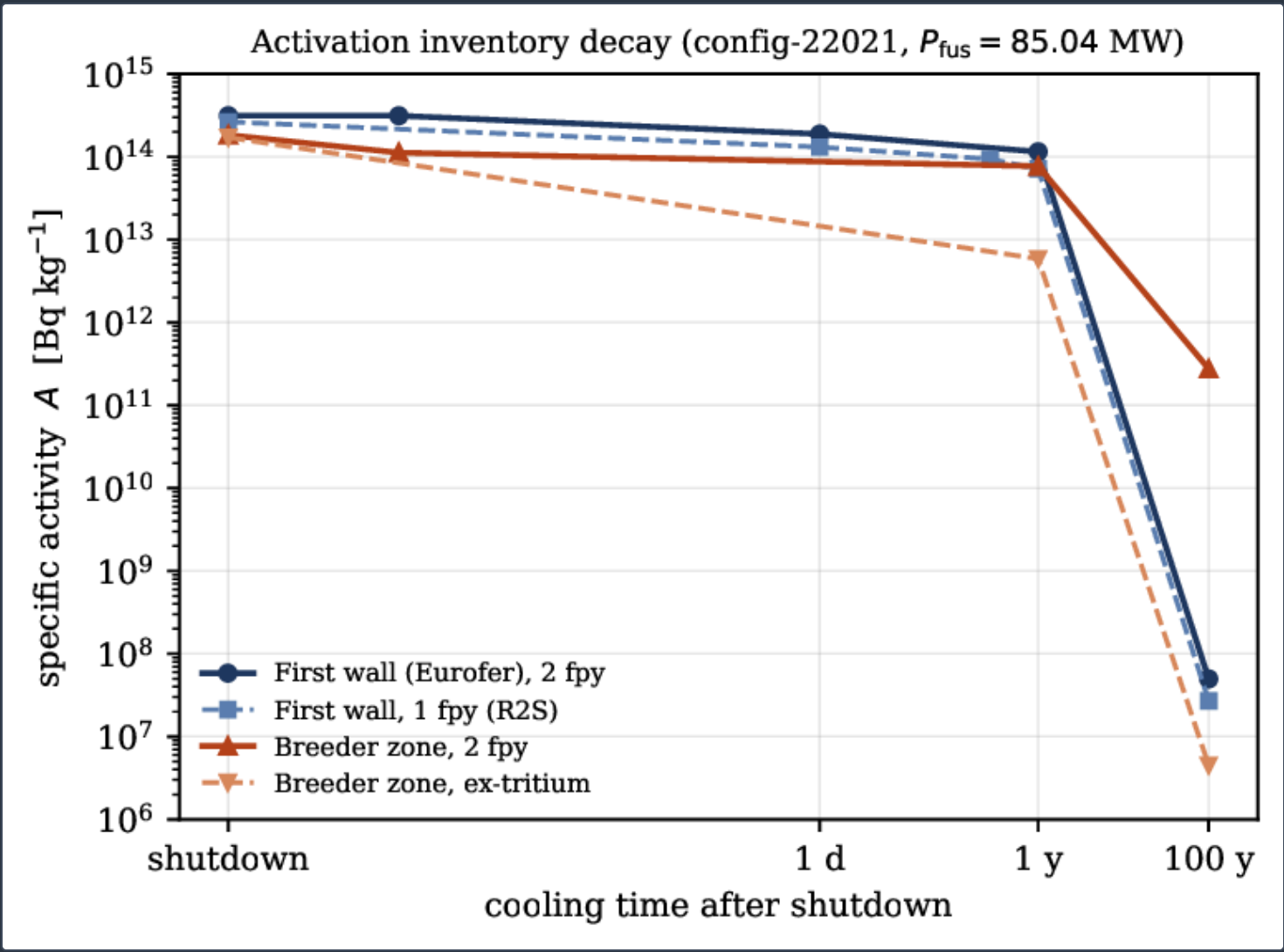

Specific-activity decay of the first wall and breeder zone after shutdown, at one- and two-full-power-year exposures (register serials BR-L1-A10, BR-L2-A23). The ex-tritium breeder-zone curve isolates the structural inventory from the bred-tritium product held in the ceramic under no-purge accounting.

STREAM	QUANTITY	SHUTDOWN	1 D	1 YR	100 YR
FW (2 fpy)	activity	3.13×10^{14}	1.88×10^{14}	1.15×10^{14}	4.97×10^{7}
FW (2 fpy)	decay heat	53.4	3.95	1.68	4.4×10^{-8}
FW (1 fpy R2S)	activity	2.64×10^{14}	1.31×10^{14}	7.13×10^{13}	2.70×10^{7}
FW (1 fpy R2S)	decay heat	56.0	2.99	1.22	2.4×10^{-8}
breeder (2 fpy)	activity	1.83×10^{14}	—	7.69×10^{13}	2.76×10^{11}
breeder (2 fpy)	decay heat	17.9	0.373	0.195	2.5×10^{-4}
breeder ex-^{3}H	activity	1.71×10^{14}	—	5.85×10^{12}	4.5×10^{6}

Specific activity and decay heat trajectories ($\mathrm{Bq\,kg^{-1}}$, $\mathrm{W\,kg^{-1}}$). FW = first wall (EUROFER-97, ex-W/Ta); breeder = ceramic-breeder zone. 2 fpy from BR-L1-A10, 1 fpy (R2S) from BR-L2-A23.

DECAY HEAT AND THE ABSENCE OF A MELT PATHWAY

Figure 4 shows the decay heat. The first-wall specific heat is 53–56 at shutdown, falling to 1.2–1.7 at one year and to $\sim 10^{-8}$ at one hundred years; the breeder zone is lower still. The bounding one-year value across the qualified HEA candidate set is ≤ 62 (Sec. 4.4). Converting to a volumetric density with EUROFER's $\rho = 7702\ \mathrm{kg\,m^{-3}}$, the shutdown decay-heat density is $q''' = \rho\dot{q} \approx 0.43\ \mathrm{MW\,m^{-3}}$, roughly two orders of magnitude below the post-shutdown decay-heat densities that drive melt in a fission core. Evaluating the passive-cooling estimates of Eqs. 9–10 with EUROFER properties ($c_p \approx 650\ \mathrm{J\,kg^{-1}\,K^{-1}}$, $\varepsilon \approx 0.3$, $L = 0.03$ m), a slab carrying the one-year $\dot{q} \leq 62$ reaches a radiative-equilibrium surface temperature of order 10^3 K — comfortably below the ~ 1800 K melting range — while by ten years $\dot{q} \sim 10^{-7}$ makes any temperature rise negligible. Because the fusion rate quenches on any excursion (no critical mass, no chain reaction) and the in-vessel fuel inventory is only seconds of burn at the $\tau_p = 2$ s particle confinement time, there is no self-sustaining heat source to outrun passive removal: the retired inventory has no meltdown pathway.

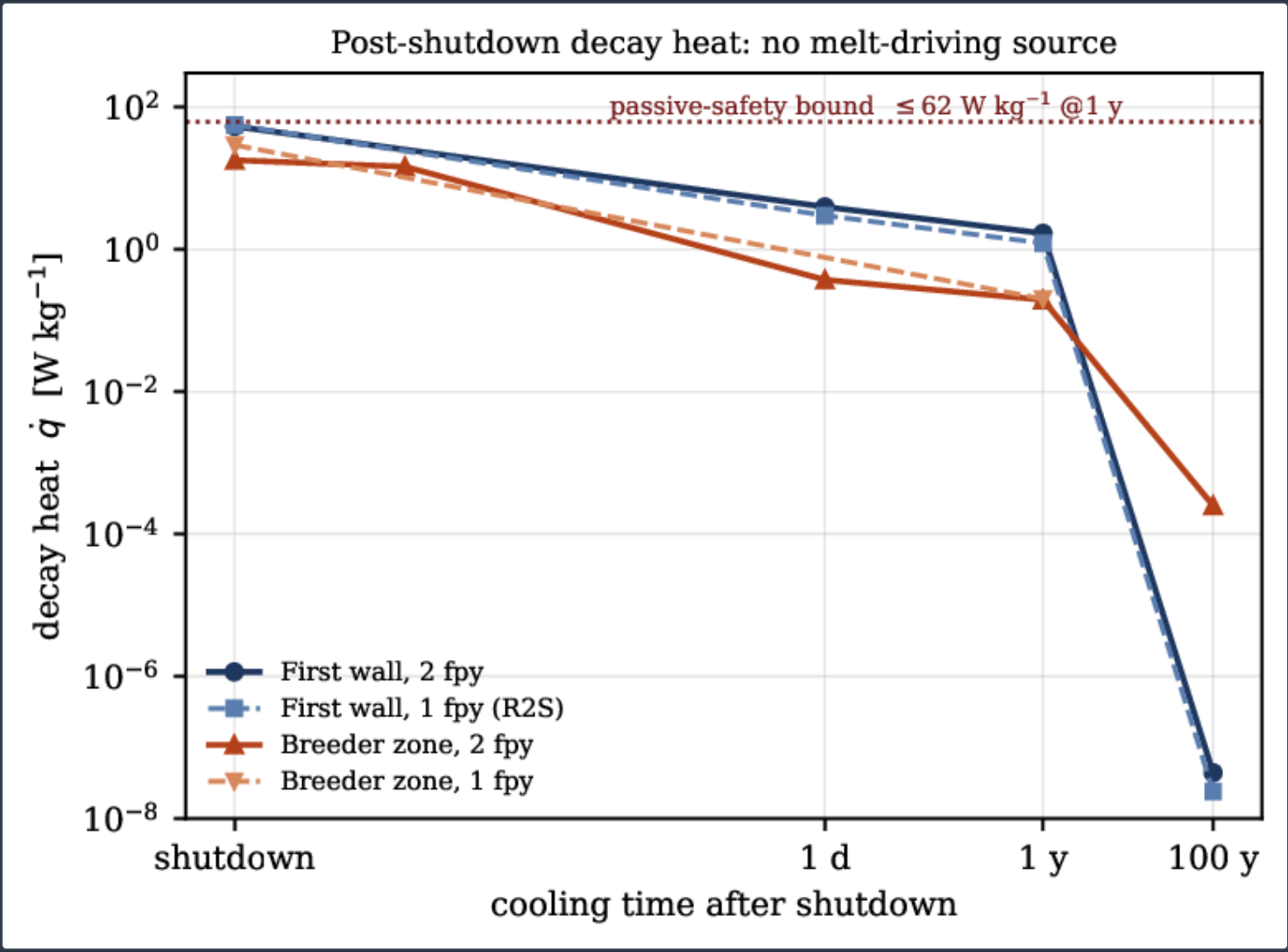

Post-shutdown decay heat of the first wall and breeder zone. The dotted line marks the ≤ 62 one-year passive-safety bound (register serial ENV-A3). The decay-heat density is two orders below fission post-shutdown values and admits no melt-driving pathway.

WASTE CLASSIFICATION: NO GREATER-THAN-CLASS-C WASTE

The classification result (Eq. 11) is the headline of the paper and is shown in Fig. 5. Every activated component classifies at or below Class C at all cooling times; nothing reaches the GTCC category that would demand deep geological disposal. The Class-C sum-of-fractions index is driven everywhere by ^{14}C and stays $\leq 2.6 \times 10^{-3}$ in both zones at every time; the largest Class-C index anywhere in the entire build is the ceramic breeder at 9.4×10^{-3}, two orders of magnitude below the $\mathcal{I}_C = 1$ boundary. The only exceedance of Class A is tritium retention: the first-wall Class-A index runs $4.96 \rightarrow 4.69$ (over 99.99% ^{3}H-driven) and the breeder Class-A index is $\sim 8.6 \times 10^{3}$ while the bred tritium is booked in place, but with tritium recovered the ex-tritium breeder index is $\sim 2.6 \times 10^{-2}$ (Class A) and the first wall clears to a Class-A index of 9.5×10^{-3} at one hundred years. In other words, *tritium management, not structural activation, sets every handling class*. Table 3 collects the indices.

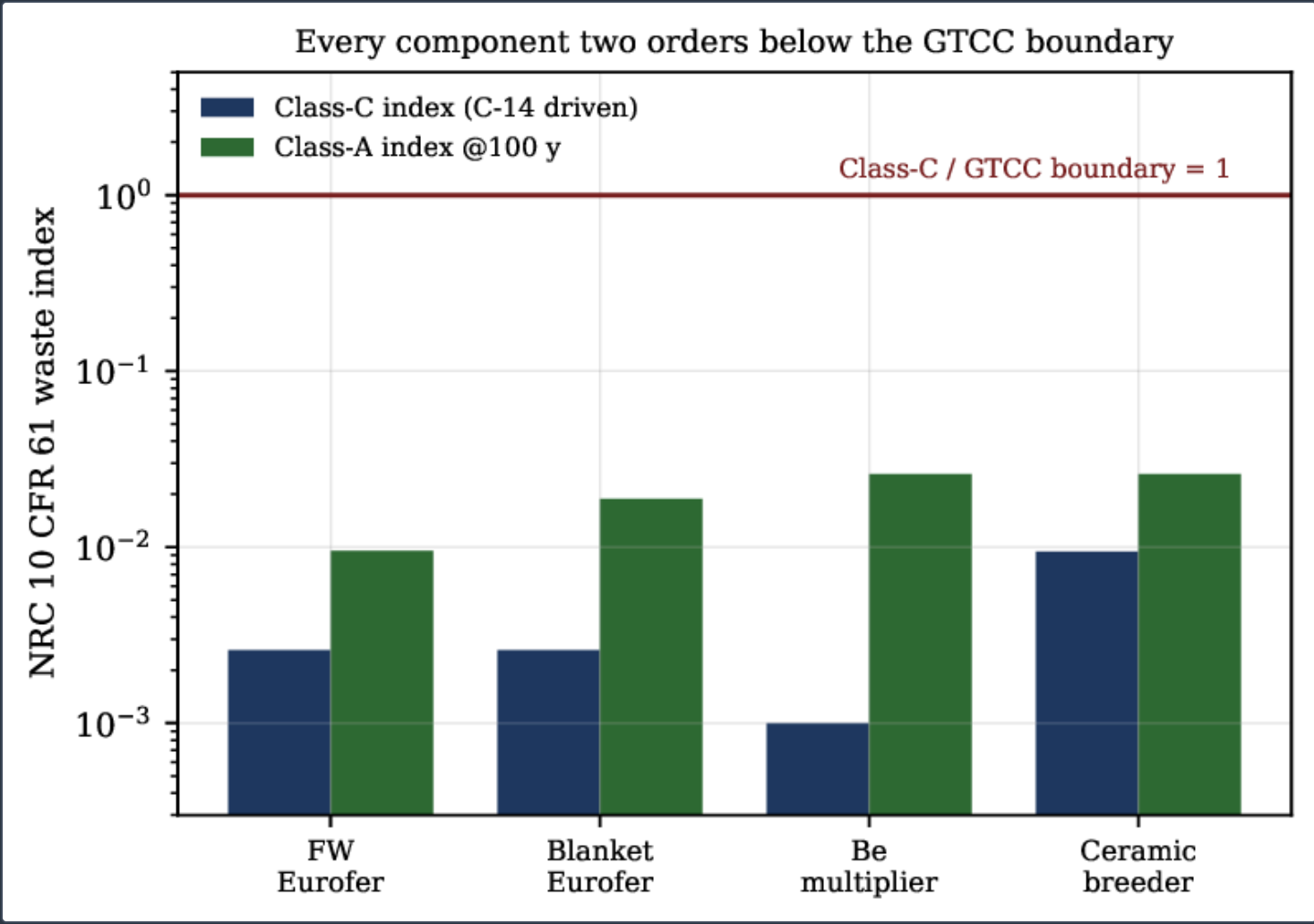

NRC 10 CFR 61 waste indices by component. The Class-C index (blue), driven by ^{14}C, is two orders of magnitude below the GTCC boundary $\mathcal{I}_C = 1$ (red line) for every component; the Class-A index after a century (green) is tritium-controlled and clears once tritium is recovered as product (register serial BR-L1-A10).

COMPONENT	CLASS-A INDEX	CLASS-C INDEX	DRIVER / NOTE
first wall (EUROFER)	$4.96 \to 4.69$ (0–1 y); 9.5×10^{-3} (100 y)	$\leq 2.6 \times 10^{-3}$	^{3}H (Class-A); ^{14}C (Class-C)
blanket EUROFER	0.47 (as-is)	$\leq 2.6 \times 10^{-3}$	Class A as-is
Be multiplier	$\sim 2.6 \times 10^{-2}$	$\sim 1 \times 10^{-3}$	Class A
ceramic breeder	8.6×10^{3} (^{3}H booked); 2.6×10^{-2} (ex-^{3}H)	9.4×10^{-3}	largest Class-C in build
4l*Result:* $\max_{\text{comp}} \mathcal{I}_{\text{C}} = 9.4 \times 10^{-3} \ll 1$; no GTCC waste; only tritium above Class A.			

Waste-detriment-response indices (10 CFR 61.55; boundary $= 1$). GTCC requires $\mathcal{I}_{\text{C}} > 1$; no component reaches it. Indices from BR-L1-A10 (2 fpy) and BR-L2-A23 (1 fpy).

WASTE ROUTING AND THE CLEARANCE TIMELINE

Classification at a single instant understates the case; the disposition of the structural stream is set by how it routes through waste classes as it cools. Figure 6 shows the descent for the qualified Kronos low-activation HEA family (candidates **L1–L4**: WTaVTi-equiatomic, a first-wall optimum, a divertor optimum, and a quinary equiatomic), evaluated at a conservatively high first-wall flux of $\mathbf{6.30 \times 10^{16}}$ ($\mathbf{4.04 \times 10^{15}}$ above **10** MeV). All four follow the same trajectory: intermediate-level (ILW) at one year (total activity $\sim \mathbf{6 \times 10^{14}}$, decay heat **51–62**), low-level (LLW) at ten years, and *clearable* at one hundred years, with a *long-lived isotopic fraction of zero at every cooling time* (Eq. 13). The one-year inventory is carried by ^{181}W, ^{182}Ta, ^{185}W and ^{46}Sc (Fig. 7) — half-lives of order months, not centuries.

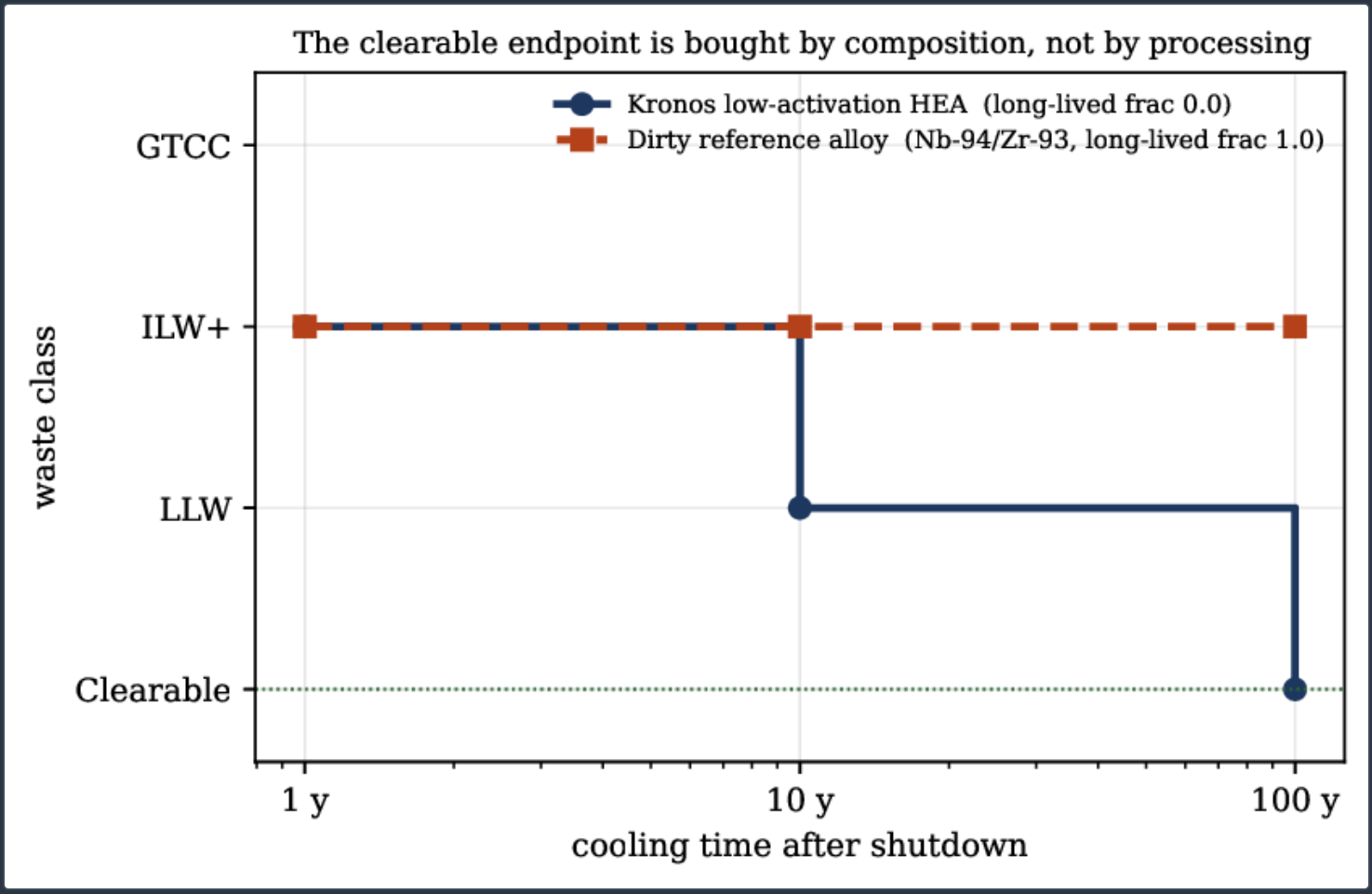

Waste-class descent of the low-activation HEA structure (register serial ENV-A2): ILW at one year, LLW at ten, clearable at one hundred, long-lived fraction **0.0** throughout. Dirty reference alloys (^{94}Nb/^{93}Zr-bearing) stay intermediate-level indefinitely with long-lived fraction **1.0**.

The contrast with conventional alloys is the whole point and is designed in, not discovered. Two “dirty” reference alloys (WTaNbMoV-equiatomic and TiZrNbMoV) processed on the identical chain stay intermediate-level at ten *and* one hundred years with a long-lived fraction approaching **1.0**, because their ^{94}Nb ($\mathbf{t_{1/2} = 2.0 \times 10^{4}}$ yr), ^{93}Zr ($\mathbf{1.5 \times 10^{6}}$ yr) and molybdenum activation products never clear (Fig. 7). The Kronos composition screen excludes Nb, Mo and Zr precisely to remove these channels, so the hundred-year clearance is *intrinsic to the material* rather than contingent on any downstream processing or dilution. This is the meaning of the paper's subtitle: with the qualified composition there is no isotope beyond a century's half-life left in the structural stream.

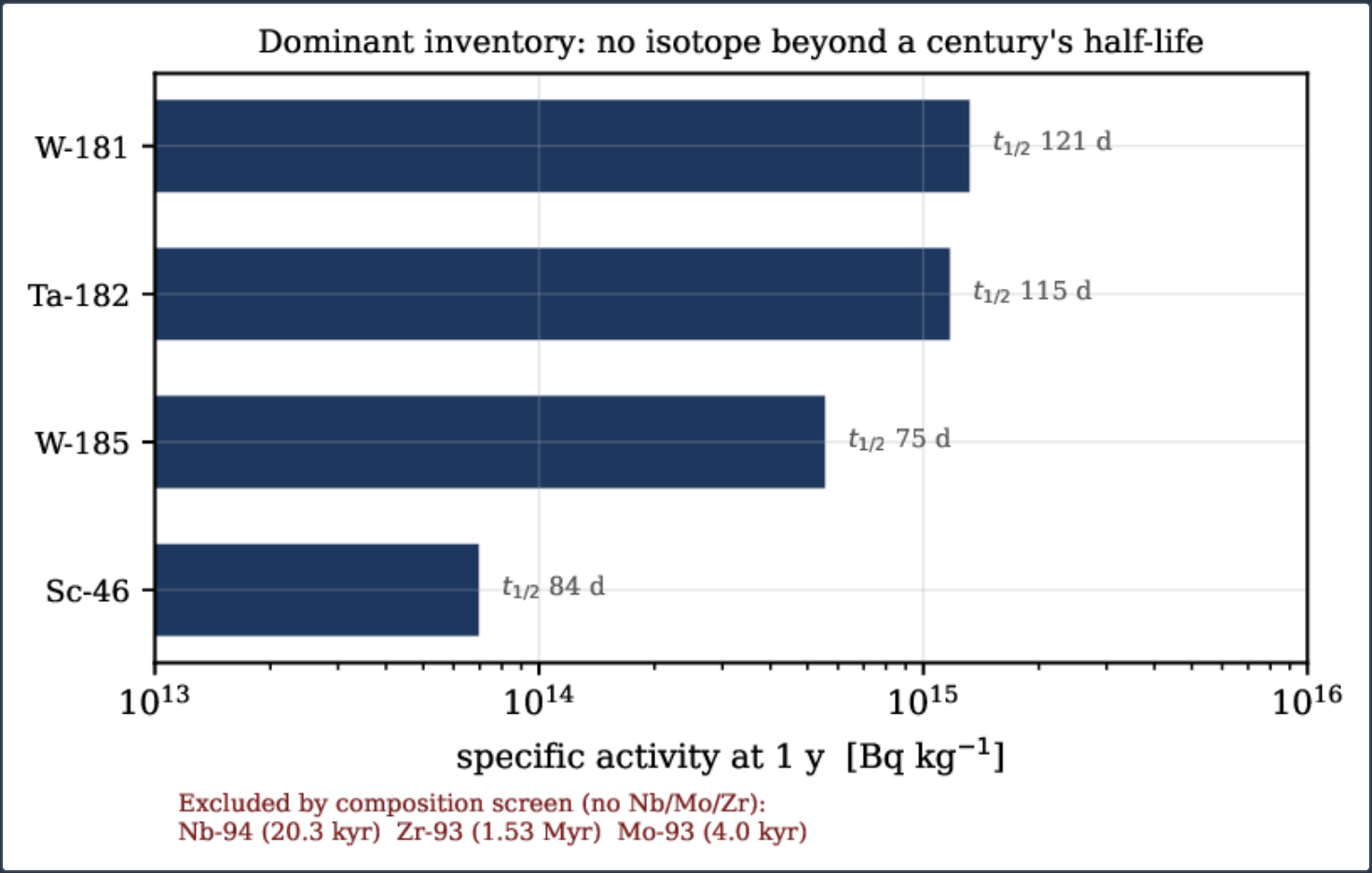

Dominant one-year specific activity of the low-activation HEA structure (register serial ENV-A2): ^{181}W, ^{182}Ta, ^{185}W and ^{46}Sc, all short/medium-lived (half-lives of months). Annotated below are the long-lived isotopes the composition screen excludes (^{94}Nb, ^{93}Zr, ^{93}Mo), which trap the dirty reference alloys above clearance indefinitely.

COOLING TIME	KRONOS HEA CLASS	DIRTY-REFERENCE CLASS	LONG-LIVED FRACTION (KRONOS)
1 yr	intermediate-level (ILW)	intermediate-level	**0.0**
10 yr	low-level (LLW)	intermediate-level	**0.0**
100 yr	clearable	intermediate-level	**0.0**

Waste routing and clearance timeline for the qualified low-activation HEA structure versus dirty reference alloys (register serial ENV-A2).

NEUTRON FIELD DRIVING THE INVENTORY

The activation inventory is only as credible as the flux that drives it. Figure 8 reports the tallied first-wall and breeder-zone fluxes on the 175-group VITAMIN-J structure, normalized to the fusion source of Eq. 3. The first-wall total is 5.628×10^{14} , with 1.071×10^{14} above 10 MeV and 17.1% of the total in the 14 MeV band — the threshold-reaction regime that produces the $(n,2n)$, (n,p) and (n,α) transmutation products. The breeder-zone flux is softer and lower, 1.302×10^{14} , consistent with moderation and absorption through the multiplier and breeder. These fluxes are the R2S source spectra for every inventory result above.

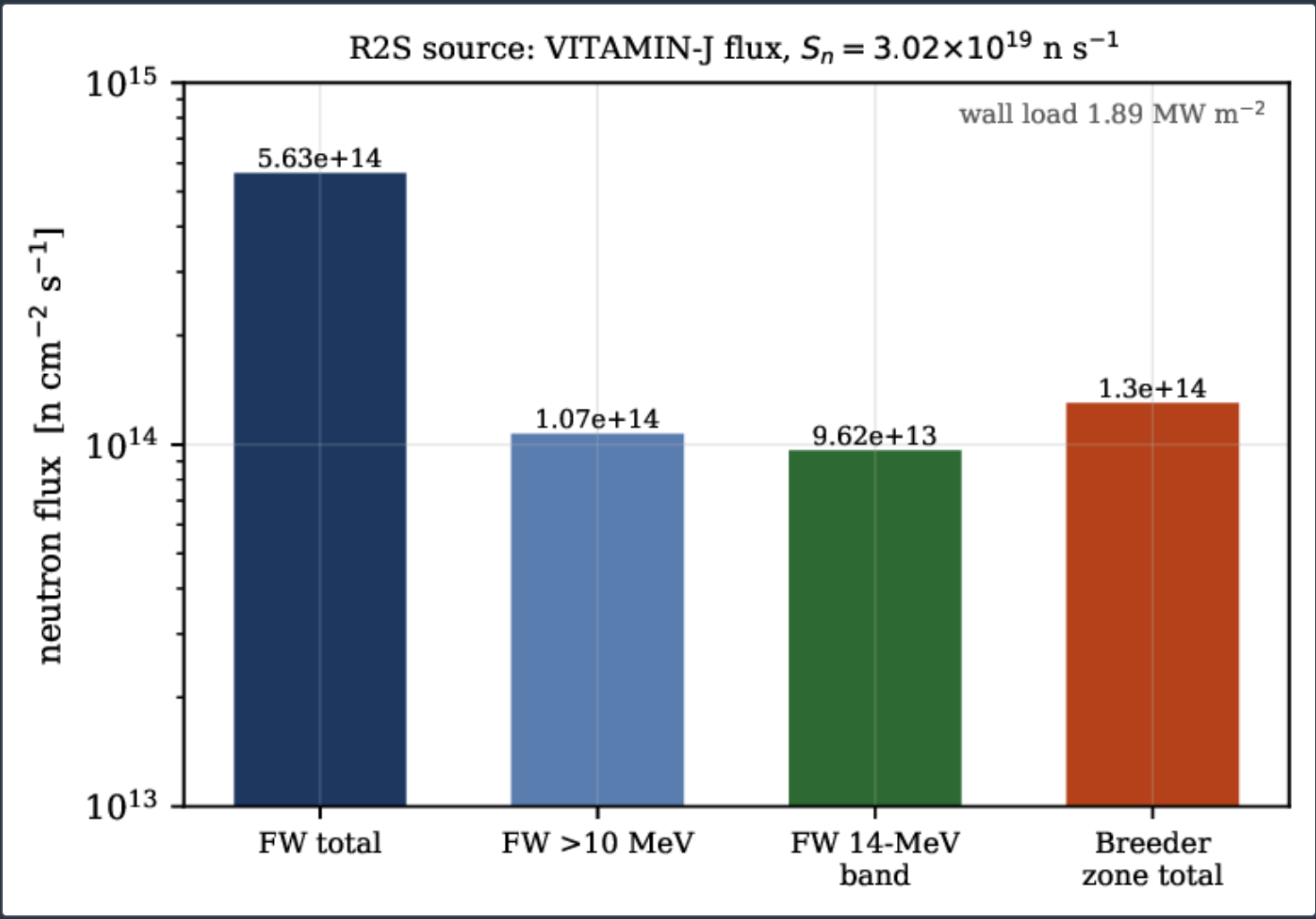

Tallied neutron flux by zone and energy band (register serial BR-L2-A23), normalized to $S_n = 3.02 \times 10^{19}$ at $P_{\text{fus}} = 85.04$ MW. The 14 MeV band drives the threshold activation reactions; the breeder-zone flux is moderated below the first-wall value.

STORED ENERGY AND THE DECOMMISSIONING FOOTPRINT

The end-of-life hazard is not only radiological. Figure 9 inventories the stored energies that could in principle drive a release. The plasma thermal energy, $W_p = \frac{3}{2}\int (n_i T_i + n_e T_e)\, dV = 16.06$ MJ, is equivalent to only ≈ 3.8 kg of TNT — a component-damage rather than off-site term. The dominant stored energy is magnetic: the field energy density $u = B^2/2\mu_0$ is $25.5\ \mathrm{MJ\,m^{-3}}$ at $B_0 = 8$ T and $112.9\ \mathrm{MJ\,m^{-3}}$ at the 16.84 T peak, giving a coil-system field energy of order 0.3 GJ over the plasma-scale volume. That energy is a quench/arc engineering hazard managed by dump resistors and structural design; it is radiologically inert. Table 5 collects these terms. The decommissioning material footprint (Fig. 10) is of order 40 t of steel and $90\ \mathrm{m^3}$ of concrete per installed megawatt at the published-LCA reference-class intensity, which for an ~ 85 MW-class breeder implies of order 3–4 kt of steel and ~ 8 kt of concrete per unit; because the structural stream clears within a century, the great majority of that mass is recyclable rather than destined for disposal, and the operation is a routine industrial one.

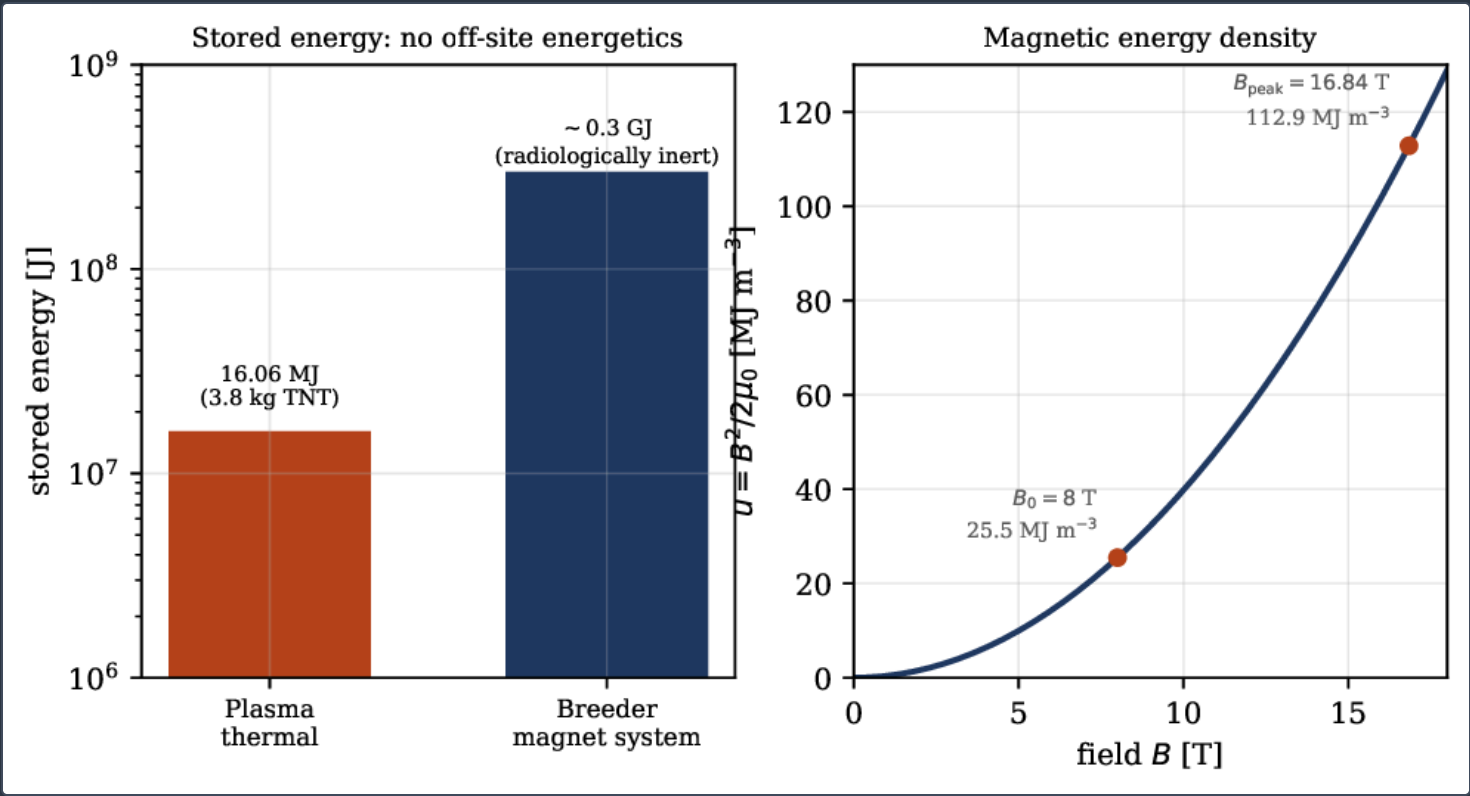

Left: stored-energy inventory (register serial ENV-A3) — 16.06 MJ plasma thermal energy (≈ 3.8 kg TNT) versus a radiologically inert ~ 0.3 GJ of coil field energy. Right: magnetic energy density $u = B^2/2\mu_0$, marked at the 8 T on-axis and 16.84 T peak-centrepost fields (two physically distinct magnet systems).

QUANTITY	VALUE	CHARACTER
plasma thermal energy W_p	16.06 MJ (≈ 3.8 kg TNT)	component-damage, not off-site
particle confinement τ_p	2 s	seconds of in-vessel fuel
$u = B^2/2\mu_0$ at 8 T	$25.5\ \mathrm{MJ\,m^{-3}}$	on-axis
$u = B^2/2\mu_0$ at 16.84 T	$112.9\ \mathrm{MJ\,m^{-3}}$	peak centrepost
coil field energy (breeder)	~ 0.3 GJ	quench/arc, radiologically inert
decay heat at 1 yr	≤ 62	no melt pathway
decay heat at 10 yr	$\sim 10^{-7}$	negligible

Stored-energy inventory and passive-safety terms (register serial ENV-A3).

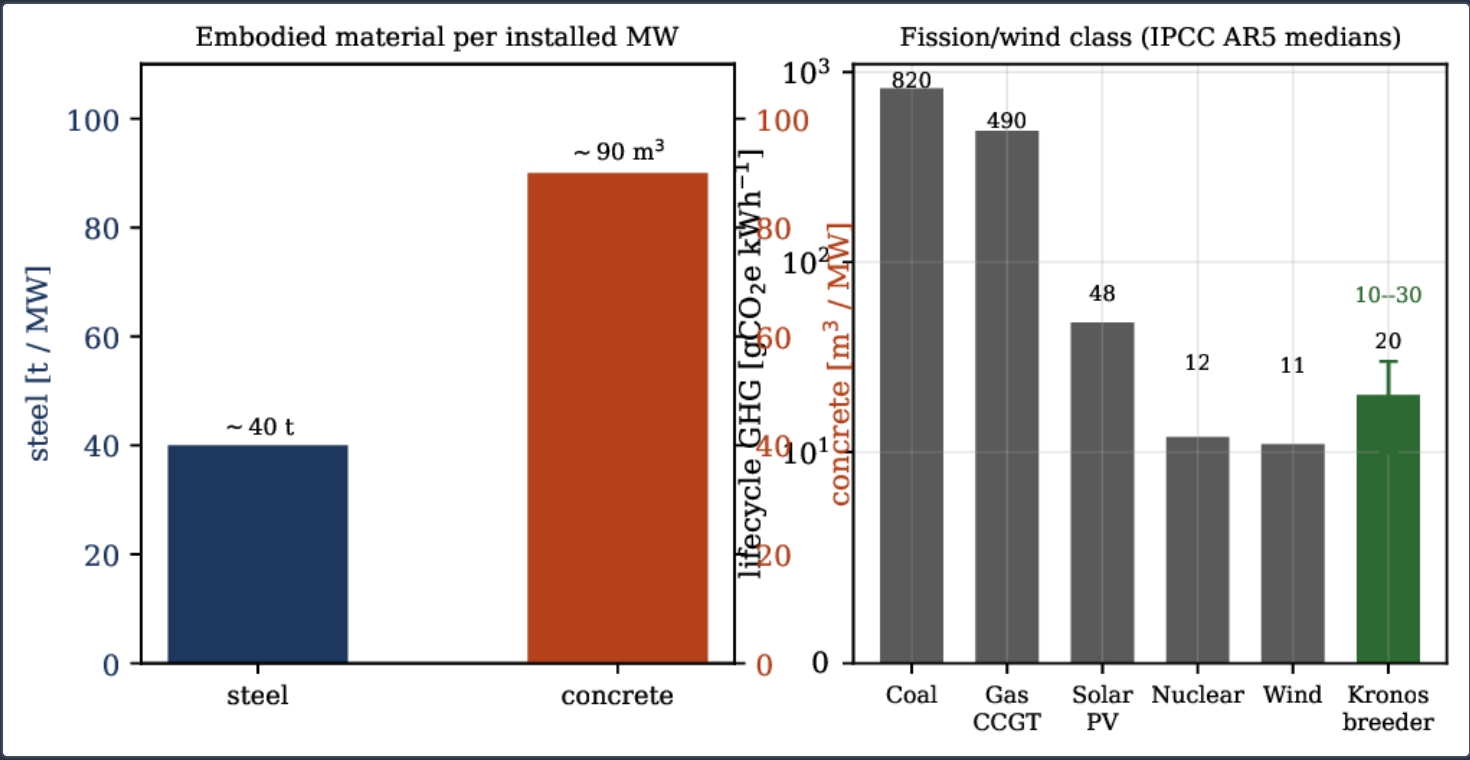

Left: embodied material footprint, of order **40** t steel and **90 m^3** concrete per installed megawatt (register serial ENV-A1; reference-class sizing proxy). Right: lifecycle greenhouse-gas intensity of the breeder, **10–30 gCO_2e kWh^{-1}**, against IPCC AR5 lifecycle medians — in the fission/wind class, dominated by embodied materials rather than operation (which is carbon-free).

FUEL AND RESOURCE FOOTPRINT

The resource draw that sustains the machine, and hence the throughput that a fleet's waste and fuel-cycle infrastructure must handle, is small. From the D–T reaction rate $R = P_{\mathrm{fus}}/Q_{\mathrm{DT}} = 3.02 \times 10^{19}$ s^{-1}, one breeder consumes **3.16 kg yr^{-1}** of deuterium and **17.1 kg yr^{-1}** of ^{6}Li (≈**225 kg yr^{-1}** of natural lithium at **7.59%** ^{6}Li abundance), burning **4.74 kg yr^{-1}** of tritium while breeding **8.53 kg yr^{-1}** for a net export of **3.79 kg yr^{-1}** — reproducing the independent toolkit value of **3.836 kg yr^{-1}** to within **1.2%** (Table 6). A canonical **∼6**-unit breeder fleet therefore draws **∼1.35 t yr^{-1}** of natural lithium against global reserves of order **26** Mt — about **5×10^{-8}** of reserves per year — while deuterium is effectively unlimited from seawater. Lithium and deuterium are non-constraints at any conceivable fleet size; the only scarce input in the wider platform is the ^{3}He that fuels the separate D–^{3}He burner, a supply question outside the breeder's waste account.

QUANTITY	VALUE	BASIS
deuterium consumed	**3.16 kg yr^{-1}**	$\dot{R} m_{\mathrm{D}}$
^{6}Li consumed	**17.1 kg yr^{-1}** (≈ **225** kg nat. Li)	breeding
tritium burned	**4.74 kg yr^{-1}**	$\dot{R} m_{\mathrm{T}}$
tritium bred	**8.53 kg yr^{-1}**	blanket
net tritium exported	**3.79 kg yr^{-1}**	vs toolkit **3.836** (**1.2%**)
∼ 6-unit fleet Li draw	**∼ 1.35 t yr^{-1}**	**5×10^{-8}** of reserves yr^{-1}

Per-breeder fuel and resource footprint (register serial ENV-A4). Reaction rate $R = P_{\mathrm{fus}}/Q_{\mathrm{DT}} = 3.02 \times 10^{19}$ s^{-1}.

§ 5

Discussion

Against published fusion activation benchmarks. The result sits squarely within, and at the favourable end of, the established fusion-activation literature. European DEMO activation and waste studies find that EUROFER-based in-vessel structures reach low-level or clearable inventories on decade-to-century timescales provided the long-lived impurity channels (^{94}Nb from Nb, ^{192m}Ir, ^{108m}Ag, and the ^{93}Mo/^{94}Nb chains) are suppressed [2,3], and consistently identify GTCC-free operation as achievable but impurity-sensitive. Our per-component indices are entirely consistent with this picture: with a W/Ta- and Nb/Mo-free composition the Class-C index is set by ^{14}C at $\leq 2.6 \times 10^{-3}$, and the residual first-wall inventory at a century ($\sim 10^{7}$) is comparable to the RAFM clearance-scale values reported for DEMO [2,5]. The distinguishing quantitative claim of this work is the *zero* long-lived isotopic fraction of the qualified HEA family (Eq. 13) — a stronger statement than "low" — which we trace directly to the first-principles composition screen that removes the offending elements at the design stage [33,34].

Waste-volume and licensing context. The absence of GTCC waste is not merely an environmental nicety; it is the technical premise of the compact breeder's licensing posture. A machine whose entire activated inventory is Class C or below, and whose dominant radiological term is a recoverable tritium product rather than a disposal liability, is the archetype the byproduct-material licensing argument rests on [39], and the century clearance timeline determines how much of the decommissioning mass returns to the material stream rather than to a repository. The shutdown-dose field that governs hands-on versus remote maintenance during that decommissioning is the R2S output of Eq. 14, developed into a spatially-resolved twin in the companion activation-twin study [35] and into duct/port occupational-dose maps in the streaming study [36].

Passive safety in context. The inherent-safety case is qualitatively different from fission's. Fission decay heat immediately after shutdown is several percent of a gigawatt-thermal rating and concentrated in a small fuel volume, requiring active, defence-in-depth cooling for days. Here the shutdown decay-heat density is $\sim 0.43\ \mathrm{MW\,m^{-3}}$ falling by four orders of magnitude within a decade, spread through the structure, and there is no critical mass to reheat it; the passive radiative balance of Eq. 10 holds the retired inventory below its melting range without intervention. The leading residual hazard is the mobile tritium inventory, a confinement design problem treated in the accident and source-term companion [38], not an energetics one.

Mass-flow and cadence. The decommissioning burden is coupled to the operational component-replacement cadence: the consumable centrepost and the plasma-facing first wall are replaced on a fluence-driven schedule set by displacement damage (of order 15.6–$23.3\ \mathrm{dpa\,fpy^{-1}}$ across the admissible current window) [37,40], so the end-of-life stream is fed incrementally over the plant life. Because each replaced component is itself GTCC-free and clears within a century, the lifetime waste ledger inherits the clean end-point of the single-shot analysis presented here.

§ 6

Limitations

The single honest gate is the first-wall activation *lower bound*. The tungsten and tantalum activation cross-sections were absent from the reduced library used for the first-wall component, so the tungsten armour was excluded and EUROFER re-normalized to exact retained number densities; the first-wall **0–10** yr activity and decay-heat figures are therefore conservative lower bounds that can only rise modestly when the W/Ta channels are restored. This does not affect the central conclusion: the Class-C index margin is two orders of magnitude, the long-lived fraction is set by the *absence* of Nb/Mo/Zr rather than by W/Ta, and completing the W/Ta activation on the same ALARA chain is the confirming calculation for the bulk-structure GTCC-free result. The lifecycle carbon and embodied-material figures are reference-class order-of-magnitude estimates (no unit-specific bill-of-materials LCA exists yet), and the hundred-year residues are reported under a no-purge tritium accounting that conservatively books bred tritium in place rather than as recovered product.

§ 7

Conclusion

The Hyperion breeder's end-of-life inventory is benign, and the finding is a computed consequence of a deliberate material choice rather than a mitigation applied afterward. A transport-driven, per-component activation calculation on the frozen $\mathbf{85.04}$ MW design point places *every activated component at or below Class C, with no greater-than-Class-C waste*; the largest Class-C index anywhere is the ceramic breeder at $\mathbf{9.4 \times 10^{-3}}$, two orders below the boundary, and only recoverable tritium pushes any stream above Class A. The qualified low-activation high-entropy-alloy structure routes cleanly from intermediate-level at one year, to low-level at ten, to *clearable* at one hundred years, with a *long-lived isotopic fraction of zero at every cooling time* — because the composition screen categorically excludes the ^{94}Nb, ^{93}Zr and molybdenum channels that trap conventional alloys above clearance indefinitely. The retired material is passively safe, with decay heat $\leq \mathbf{62}$ at one year and no melt pathway; the stored energies are small ($\mathbf{16.06}$ MJ plasma, $\sim\mathbf{0.3}$ GJ radiologically inert coil field); and decommissioning handles a modest, largely recyclable footprint of order $\mathbf{40}$ t steel and $\mathbf{90\,m^3}$ concrete per megawatt at a $\mathbf{10}$–$\mathbf{30\ gCO_2e\,kWh^{-1}}$ lifecycle intensity. No isotope in the structural stream survives beyond a century's half-life. The waste case is closed.

Acknowledgments tocsectionAcknowledgments Part of the Kronos Fusion Energy 2026 design series. The activation and waste results were produced and independently re-run on the Kronos NVIDIA GPU HPC campaign; the authors thank the de-risking programme for the frozen-anchor regression suite that underlies the reproducibility of these results.

Reproducibility. The activation inventory, waste-class timeline, decay-heat, stored-energy, footprint and fuel-balance results are frozen results in the Kronos Physics De-Risking Register (serials BR-L1-A10, BR-L2-A23, ENV-A1, ENV-A2, ENV-A3, ENV-A4), regenerable from the archived transport tallies and ALARA/FISPACT inventory decks under fixed seed `20260726` on the config-22021 design point. This paper is archived at doi:10.5281/zenodo.22645846; official version: https://www.kronosfusionenergy.com/publications/component-activation-waste-class-routing-and-decommissi.html and the register at doi:10.5281/zenodo.22133057.

Data availability tocsectionData availability This paper is archived at doi:10.5281/zenodo.22645846. The activation-inventory, waste-classification, clearance-timeline and footprint tables are archived with the deposit and reference the Kronos 2026 series. Any economic analysis is reported separately and is not part of the public deposit.

Competing interests tocsectionCompeting interests Provisional patent applications relating to aspects of the low-activation alloy family and its manufacture have been filed. The authors declare no other competing interests.

Portfolio, People & Record

The intellectual-property estate, the people who built it, the limitations that gate it, and the sources it rests on.

1	4	40	27
GRANTED PATENT	2026 PROVISIONALS	TEAM MEMBERS	2022 PROVISIONALS

INTELLECTUAL PROPERTY

The patent portfolio

The estate spans a granted high-field magnet patent, pending utility and 2026 provisional filings that map to the two products, a digital-twin control provisional, a registered trademark application, and the original 2022 provisional family. Every patentable disclosure in the five-paper arXiv drop was protected **before** publication: the breeder and burner provisionals were filed 1–2 August, and a publication-gap omnibus filing the evening before the drop swept up the DEC, plasma-control, and REBCO-winding matter of the three otherwise-unprotected papers. Patent numbers and application serials are matters of public record; claim scope is summarised, not reproduced.

GRANTED & PENDING UTILITY

US 12,009,112	High-field tilted graded-REBCO magnet architecture (KRONO-002A) · *app. 17/878,550*	GRANTED
US 17/878,507	Core device / method (KRONO-001A) · *utility*	PENDING

2026 PROVISIONAL FILINGS — MAPPED TO THE PRODUCTS

64/124,209	Hyperion — spherical-tokamak tritium / helium-3 foundry · *breeder · filed Aug 2026*	FILED
64/124,220	Aegis / MetroVolt — synchrotron-cutoff, fuel-selection & plug-winding · *generator · filed Aug 2026*	FILED
64/115,167	KRONOS-CTRL digital-twin plant control · *provisional · filed Jul 2026*	FILED
64/005,440	Integrated spherical-tokamak fusion architecture · *early integrated-architecture filing · filed Mar 2026*	FILED
64/105,530	Negative-triangularity spherical-tokamak architecture · *foundational ST filing · filed Jul 2026*	FILED
64/128,097	Publication-gap omnibus — quasineutral two-species expander DEC · provenance-gated / latency-split plasma control · as-built high-field winding & conductor architecture · *filed 7 Aug 2026, the evening before the arXiv drop*	FILED

TRADEMARK & ORIGIN

FTK-98801894	Kronos Fusion Energy — trademark application	FILED
KR-2022-*	Original provisional family (KR-2022-00001 … 00027) · *27 filings, 2022*	PRIORITY

The narrow, defensible magnet novelty — the specific conductor and the digital-twin winding optimisation, not high-field REBCO as a category — is the commercial core that can earn ahead of any Q > 1 milestone, with markets in fusion magnet supply, MRI/NMR, accelerators, and proton therapy. The claim is scoped honestly: the high field is a *system field* result, not a stand-alone-coil record; the small-bore plug coil is structurally infeasible as a bare winding but resolved by a stress-managed structural shield (feasible-pending-FEA); and the winding-tape experiment returned a *null result*. The value is the method, not a field record.

THE TEAM

Founding partners, board, advisors & auditors

Kronos is built by a bench of advanced-fuel-fusion, high-field-magnet, direct-conversion, and materials specialists, with a board and operations team drawn from defense, national laboratories, and industry. Dates are shown as ranges; where a tenure has ended or is term-ending, the range says so.

FOUNDING PARTNERS — SCIENCE

Dr. Gerald Kulcinski
Co-Founder · Helium-3 & Advanced-Fuel Fusion
UW–Madison · 2023–Present

Dr. Carl Weggel
Chief Scientist / S.M.A.R.T. Design
MIT Alcator Program · 2022–Present

Dr. Robert J. Weggel
Magnetic Field Design
MIT Magnet Lab · 2022–Present

BOARD

Priyanca Ford
Founder & CEO · Executive Board
2022–Present

Bandel Carano
Finance / Strategy
Oak Investment Partners / Stanford · 2025–2026

Patrick Schweiger
Fusion Device Engineering
Oklo / CFS / TerraPower · 2025–Present

SCIENTIFIC ADVISORS

Dr. Steven O. Dean
Fusion Policy & History
DOE / Fusion Power Associates · 2025–Present

Dr. Patrick H. Diamond
Plasma Turbulence & Transport
UC San Diego · 2025–Present

Dr. Jack J. Dongarra
HPC & Numerical Algorithms
Turing Award · 2025–Present

Dr. Nasr M. Ghoniem
Chief Material Scientist
UCLA · 2025–Present

Dr. Siegfried Glenzer
Plasma Physics & Laser Fusion
Stanford / SLAC · 2022–Present

Dr. David A. Hammer
Pulsed-Power Fusion
Cornell · 2025–Present

Dr. Donald A. Spong
Plasma Theory & Confinement
ORNL · 2025–Present

Dr. Curtis Smith
Risk Assessment & Nuclear PRA
MIT / Idaho National Lab · 2025–Present

RADM (Ret.) David Goggins
Naval Engineering & Power-Plant Design
U.S. Navy · 2023–2026

Dr. Konstantin Batygin
Mathematician
Caltech · 2022–2025

Dr. Ruben Fair
Magnet Design / ITER Liaison
PPPL / Jefferson Lab · 2022–2025

Dr. Paul S. Weiss
Materials & Nanotechnology
UCLA · 2022–2025

SCIENTIFIC AUDITORS

Dr. Wilfred A. Cooper
Plasma Equilibrium Theory
EPFL / Swiss Plasma Center · 2025–Present

Dr. Ahmed Hassanein
Plasma–Material Interactions
Purdue / Argonne · 2025–Present

Dr. Patrick E. Hopkins
Extreme Thermal Materials
U. of Virginia · 2025–Present

Dr. Peter Hosemann
Materials Joining & Structural Integrity
UC Berkeley · 2025–Present

Dr. Travis W. Knight
Advanced Nuclear Fuels & Systems
U. of South Carolina · 2025–Present

Dr. Philippe Lebrun
Cryogenics & Magnet Cooling
CERN · 2025–Present

Dr. Nitendra Singh
Nuclear Safety & Fuel Cycle
ITER · 2025–Present

Dr. Guido Van Oost
Magnetic Confinement & Fusion Systems
Ghent University · 2025–Present

Dr. Gary S. Was
Radiation Materials & Structural Integrity
U. of Michigan · 2025–Present

Dr. Ray Sedwick
Direct Energy Conversion
U. of Maryland · 2025

OPERATIONS

Michael Laughlin
Chief Operating Officer
2022–Present

Martin Owens
Chief Strategy Officer
LANL / GE Hitachi · 2022–Present

MG (Ret.) Paul Pardew
Chief Contracting Officer
Army Contracting Command · 2022–Present

David Beck
Fusion Commercialization
U.S. Space Force · 2024–Present

Sushma Bhatia
Environmental & Legislative
Google · 2022–Present

Michael De Frenza
Technology Licensing
2023–Present

MG (Ret.) Robin L. Fontes
Cybersecurity & Defense
Army Cyber Command · 2022–Present

Vijay Gehani
Supply Chain & Components
INOX India · 2024–Present

Jon Michel Greenwood
IT & AI Infrastructure
Live Nation · 2023–Present

Brian C. O'Neill
National Security
CIA / ODNI · 2022–Present

Gen. (Ret.) Gustave F. Perna
DoD Liaison
Operation Warp Speed · 2022–2023

Andrea Romero
Marketing Lead
2022–Present

Legal counsel is retained; those roles are held on the internal roster and are not listed here.

SOURCES

References

1 P I Ford, *The Physics De-Risking Register: Gate-by-Gate Evidence, Independently Re-Run and Stamped, Across a Compact Spherical-Tokamak Breeder and Its D–^{3}He Tandem-Mirror Burners*, Kronos Fusion Energy 2026 series. doi:10.5281/zenodo.22133057

2 M R Gilbert, T Eade, C Bachmann, U Fischer and N P Taylor, Waste implications from minor impurities in European DEMO materials, *Nucl. Fusion* **59** 076015 (2019).

3 M R Gilbert, S L Dudarev, S Zheng, L W Packer and J-Ch Sublet, An integrated model for materials in a fusion power plant: transmutation, gas production and helium embrittlement under neutron irradiation, *Nucl. Fusion* **52** 083019 (2012).

4 N Taylor and P Cortes, Lessons learnt from ITER safety & licensing for DEMO and future nuclear fusion facilities, *Fusion Eng. Des.* **89** 1995 (2014).

5 N P Taylor and R Pampin, Activation properties of tungsten as a first wall protection in fusion power plants, *Fusion Eng. Des.* **81** 1333 (2006).

6 J-Ch Sublet, J W Eastwood, J G Morgan, M R Gilbert, M Fleming and W Arter, FISPACT-II: an advanced simulation system for activation, transmutation and material modelling, *Nucl. Data Sheets* **139** 77 (2017).

7 P P H Wilson and D L Henderson, *ALARA: analytic and Laplacian adaptive radioactivity analysis*, University of Wisconsin Fusion Technology Institute report UWFDM-1070 (1998).

8 P K Romano, N E Horelik, B R Herman, A G Nelson, B Forget and K Smith, OpenMC: a state-of-the-art Monte Carlo code for research and development, *Ann. Nucl. Energy* **82** 90 (2015). doi:10.1016/j.anucene.2014.07.048

9 D A Brown *et al*, ENDF/B-VIII.0: the 8th major release of the nuclear reaction data library with CIELO-project cross sections, new standards and thermal scattering data, *Nucl. Data Sheets* **148** 1 (2018). doi:10.1016/j.nds.2018.02.001

10 T J Tautges, P P H Wilson, J Kraftcheck, B F Smith and D L Henderson, Acceleration techniques for direct use of CAD-based geometries in Monte Carlo radiation transport, *Int. Conf. on Mathematics, Computational Methods & Reactor Physics (M&C 2009)*, Saratoga Springs (2009).

11 M Pusa and J Lepp\"anen, Computing the matrix exponential in burnup calculations, *Nucl. Sci. Eng.* **164** 140 (2010).

12 H Bateman, The solution of a system of differential equations occurring in the theory of radioactive transformations, *Proc. Cambridge Philos. Soc.* **15** 423 (1910).

13 U.S. Nuclear Regulatory Commission, *10 CFR 61.55 — Waste classification*, Code of Federal Regulations, Title 10 (Licensing Requirements for Land Disposal of Radioactive Waste).

14 S Fetter, E T Cheng and F M Mann, Long-term radioactive waste from fusion reactors: part II, *Fusion Eng. Des.* **13** 239 (1990).

15 International Atomic Energy Agency, *Application of the Concepts of Exclusion, Exemption and Clearance*, IAEA Safety Standards Series No. RS-G-1.7, Vienna (2004).

16 R Lindau *et al*, Present development status of EUROFER and ODS-EUROFER for application in blanket concepts, *Fusion Eng. Des.* **75–79** 989 (2005).

17 E E Bloom, The challenge of developing structural materials for fusion power systems, *J. Nucl. Mater.* **258–263** 7 (1998).

18 S J Zinkle and J T Busby, Structural materials for fission & fusion energy, *Mater. Today* **12** 12 (2009).

19 N Baluc *et al*, Status of reduced activation ferritic/martensitic steel development, *J. Nucl. Mater.* **367–370** 33 (2007).

20 O El-Atwani *et al*, Outstanding radiation resistance of tungsten-based high-entropy alloys, *Sci. Adv.* **5** eaav2002 (2019). doi:10.1126/sciadv.aav2002

21 E P George, D Raabe and R O Ritchie, High-entropy alloys, *Nat. Rev. Mater.* **4** 515 (2019). doi:10.1038/s41578-019-0121-4

22 B Cantor, I T H Chang, P Knight and A J B Vincent, Microstructural development in equiatomic multicomponent alloys, *Mater. Sci. Eng. A* **375–377** 213 (2004).

23 M J Norgett, M T Robinson and I M Torrens, A proposed method of calculating displacement dose rates, *Nucl. Eng. Des.* **33** 50

COLOPHON

How this document was made

The Kronos Fleet — Combined Editorial, 2026 is set in **Fraunces** (display), **Gelasio** (text), and **IBM Plex Mono** (data & equations), carried forward from the Kronos editorial design system.

The figures are rendered at 300 dpi from the deposited generator scripts; the document is composed as a single self-contained file with embedded fonts and imagery, paginated to US Letter, and rendered to PDF through a headless Chromium engine in matched light and dark editions.

Every headline quantity carries an evidence class; withdrawn and restated values are marked as such. Nothing herein is frozen beyond the founder-approved Tier-A set.

Explore it live — turn the interactive 3-D model, run the deposited solvers in the physics validator, and watch the companion film series.

◆

LEGAL NOTICE

Notice, status, and distribution

Conceptual design & simulation study. This document reports a conceptual design and simulation study. It is not a construction commitment, a safety-analysis report, a regulatory filing, or an offer of securities. Forward-looking statements — schedules, costs, market sizes, and performance — are estimates subject to the limitations set out in the Simulations part and may change.

Numbers and their classes. Quantities are reported with evidence classes and case labels; modelled, assumed, and requirement-class values are identified as such and are not to be quoted without their labels.

Public edition. This edition carries the physics and design only; all financial, funding, and defense-commercial content has been removed for public distribution. The scientific text corresponds to the arXiv and journal submissions.

THE 2026 KRONOS SERIES

One programme, many papers

This editorial is one paper in the Kronos 2026 series — a real fusion company's complete, reproducible physics record for a spherical-tokamak breeder and its low-neutron D–^{3}He tandem-mirror burners. Every headline number is a frozen anchor in the Physics De-Risking Register.

Explore the whole programme: the De-Risking Register, the interactive 3-D model, and the physics validator.

KRONOS FUSION ENERGY

Component Activation, Waste-Class Routing, and Decommissioning of a Low-Activation Compact Spherical-Tokamak Breeder: No Isotope Beyond a Century's Half-Life

A real fusion company building real machines. Explore the science, live.

Zenodo · doi:10.5281/zenodo.22645846

Read on kronosfusionenergy.com

The Physics De-Risking Register